ELSEVIER

Polymer 42 (2001) 8137–8151

polymer

www.elsevier.nl/locate/polymer

Solid-state ^{1}H-static, ^{1}H-MAS, and $^1H \rightarrow {}^{19}F/{}^{19}F \rightarrow {}^1H$ CP/MAS NMR study of poly(vinyl fluoride)

Shinji Ando[a,*], Robin K. Harris[b], Peter Holstein[c], Stefan A. Reinsberg[b,1], Kazuo Yamauchi[d]

[a]*Department of Organic and Polymeric Materials, Tokyo Institute of Technology, Ookayama, Meguro-ku, Tokyo 152-8552, Japan*
[b]*Department of Chemistry, University of Durham, South Road, Durham DH1 3LE, UK*
[c]*Sinus-Messtechnik GmbH, Foepplstr., Leipzig 04347, Germany*
[d]*Bruker Japan Co. Ltd., Ninomiya, Tsukuba-shi, Ibaraki 305-0051, Japan*

Received 26 December 2000; received in revised form 5 April 2001; accepted 23 April 2001

Abstract

Solid-state $^1H \rightarrow {}^{19}F$-CP/MAS, $^{19}F \rightarrow {}^1H$ CP/MAS, and ^{1}H fast MAS NMR spectra have been investigated for a semicrystalline polymer, namely poly(vinyl fluoride) (PVF), together with its solution-state ^{19}F spectrum and static solid-state ^{1}H pulsed and broad line NMR measurements. The static ^{1}H pulsed NMR measurements of $T_{1\rho}^{H}$ and T_2^{H} showed the two-phase (immobile and mobile) nature, and the Goldman–Shen type phase selection at 130°C indicated that a measure for the lamellar size yields about 4.2 nm. Although the solid-state ^{19}F-CP/MAS spectrum shows a featureless lineshape, the mobile region was selectively observed by a newly developed DIVAM pulse sequence. Solid-state spin-lock experiments showed significant differences in $T_{1\rho}^{F}$ and $T_{1\rho}^{H}$ between the immobile and mobile regions, and the effective time constants, T_{HF}^{*} and $T_{1\rho}^{*}$, which were estimated from the $^1H \rightarrow {}^{19}F$ CP curves, also clarify the difference in the strengths of dipolar interactions. Furthermore, the $^1H \rightarrow {}^{19}F$ inversion recovery CP (IRCP) experiment was more advantageous in observing the relatively weak dipolar interactions in the mobile region. The inverse $^{19}F \rightarrow {}^1H$ CP/MAS and $^1H \rightarrow {}^{19}F$ CP-drain MAS experiments gave complementary information to the $^1H \rightarrow {}^{19}F$ CP/MAS spectra, although spinning at 35 kHz is necessary to separate the signals between CHF and CH_2 protons in the ^{1}H spectra. The hetero-nuclear dipolar oscillation behaviours and the effective time constants, T_{HF}^{*}, T_{FH}^{*}, and $T_{1\rho}^{*}$ determined from the $^1H \rightarrow {}^{19}F$ CP/MAS, CP-drain MAS, and $^{19}F \rightarrow {}^1H$ CP/MAS experiments are consistent with each other. In addition, the value of N_F/N_H (N is a spin density) estimated from the CP-drain curve is equivalent to that calculated from the chemical structure. © 2001 Elsevier Science Ltd. All rights reserved.

Keywords: CP-MAS NMR; Poly(vinyl fluoride); Phase structure

1. Introduction

High-speed magic-angle spinning (MAS) and high-power decoupling techniques facilitate the measurement of high-resolution solid-state ^{19}F and ^{1}H-NMR spectra for proton-containing fluoropolymers. Several papers have reported ^{19}F spectra involved in analysis of chemical structures and phase structures of solid fluoropolymers [1–7] and other fluorine-containing solids [8–10]. Recently, we have reported the characteristic features of CP dynamics between ^{19}F and ^{1}H using $^1H \rightarrow {}^{19}F$ and $^{19}F \rightarrow {}^1H$ CP/MAS NMR for a fluorinated polyimide [11] and a Viton-type fluoroelastomer [12]. The analysis was based on a phenomenological approach for the spin thermodynamics between two spin baths, but the high abundance of fluorine atoms and efficient $T_{1\rho}^{H}$ process were explicitly considered. The values of $T_{1\rho}^{H}$ and $T_{1\rho}^{F}$ obtained by the simultaneous fitting of the evolution of magnetisation in the standard CP and a modified CP (TORQUE) experiment, using the exact solutions of the equations for the spin thermodynamics, are consistent with those independently measured by spin-locking experiments.

Poly(vinyl fluoride) (PVF) is a semicrystalline fluoropolymer having high resistance to weathering. The random nature of vinyl fluoride monomer addition in radically polymerized PVF is known to give an atactic configuration and a substantial proportion of regio-irregular structure, i.e. head-to-head and tail-to-tail (HH/TT) linkages. However, the defects in the chemical structure do not prevent the polymer from crystallizing. It has been reported that the crystallinities of PVF are as high as 60% [13], and the crystalline region contains ca. 20% HH linkages (from X-ray diffraction data [14]). Two types of X-ray analyses showed that

---

[*] Corresponding author. Tel.: +81-3-5734-2137; fax: +81-3-5734-2889. *E-mail address:* sando@polymer.titech.ac.jp (S. Ando).

[1] Present address: Max-Planck-Institut für Polymerforshung, Ackermannweg 10, D-55128 Mainz, Germany.

PII: S0032-3861(01)00303-2

PVF crystallises in a disordered manner [14]. The unit cell dimensions indicate that there is a mirror-plane perpendicular to both the *a*- and *c*-axes with a two-fold rotation axis parallel to the *b*-direction. The *c*-spacing (2.52 Å) implies an extended planar zig-zag conformation of the chains. This situation is quite different from that of poly(vinylidenefluoride) (PVDF), for which five crystalline modifications have been reported, resulting in a complicated physical microstructure. The most important polymorphs of PVDF are the α-phase (t–g^+–t–g^- conformation) and β-phase (all-*trans* conformation), and numerous modes of interconversions between the modifications have been discovered. On the other hand, such variations in modification have never been reported for PVF. Hence, we assume in this study that the polymer chains of PVF take the all-*trans* conformation in the crystalline region, whereas variations in conformation may exist in the amorphous phase. This situation results in higher molecular mobility for the latter than for the former. The glass transition temperature (T_g) of the polymer has been reported as 41°C by thermal mechanical analysis [15]. We report here the investigation of ^{1}H → ^{19}F CP/MAS, ^{19}F → ^{1}H CP/MAS, ^{1}H → ^{19}F CP-drain/MAS and ^{1}H fast MAS NMR spectra of PVF in the solid state together with its solution-state ^{19}F spectrum and static solid-state ^{1}H pulsed and broad line NMR measurements. To our knowledge, PVF has never been investigated by high-resolution solid state ^{19}F and ^{1}H-NMR.

2. Experimental

2.1. Sample

Poly(vinyl fluoride) film of commercial origin, which was purchased from Goodfellow (Cambridge, England), was used for this work. The film was dissolved in *N*,*N*-dimethylformamide (DMF) at 110°C (ca. 5 wt%) and then slowly poured into methanol. The precipitated solid was dried under vacuum at 110°C for 4 h in order to evaporate absorbed solvent and ground into powder prior to being packed in the rotor.

2.2. Nuclear magnetic resonance

Solid-state MAS NMR experiments were carried out on a Chemagnetics CMX-200 spectrometer except for the ^{1}H fast MAS measurement. The spectrometer operated at resonance frequencies of 188.288 MHz for fluorine and 200.13 MHz for protons. The experimental details have been reported elsewhere [11,12]. Samples were spun at the magic angle at a rate of 13.5 kHz. The fluorine and proton RF fields were adjusted to fulfil the Hartmann–Hahn (H–H) condition: $|\omega_{1F}|/2\pi = |\omega_{1H}|/2\pi = 83$ kHz. Although the signals obtained at the H–H condition were weaker than those at the sidebands, the RF power in the proton channel was set to the centreband prior to the experiments in order to apply the simple forms of spin-thermodynamics theory [11]. The CP experiments were carried out at ambient probe temperature. The temperature inside the rotor, which was calibrated via replacement with a sample of methanol absorbed on tetrakis(trimethylsilyl)silane at the same spinning rate [16], was 35°C. Fluorine chemical shifts are quoted with respect to the signal for CFCl$_3$ and were measured via replacement with a sample of liquid C$_6$F$_6$ (−164.3 ppm) without proton decoupling. Relaxation delays of 3.5 s are sufficiently long compared with the spin–lattice relaxation time in the laboratory frame of the sample ($T_1^F = 0.5$ s, $T_1^H = 0.4$ s) to ensure quantitative peak intensities. The pulse sequences for the standard variable contact time ^{1}H → ^{19}F CP experiment, the inversion recovery ^{1}H → ^{19}F CP (IRCP) experiment, and the ^{1}H → ^{19}F CP-drain experiment [11] are depicted in Fig. 1a–c. The IRCP experiment consists of a standard CP period with a relatively short contact time followed by a sudden phase reversal in the fluorine channel (inverse CP). Since the spin temperature of the fluorines is inverted, the fluorine magnetisation is progressively inverted during the contact time, t_{CP}, in which the signal goes through zero at a definite time. The CP-drain experiment is used to measure the contact time dependence of the residual H magnetisation during the ^{1}H → ^{19}F CP experiment. The ^{1}H magnetisation is first generated by ^{19}F → ^{1}H CP with a standard contact time (0.5 ms). After the CP, the magnetisation is retained by spin-locking for 4 ms. During this spin-lock time, the residual fluorine magnetisation dephases completely. Subsequently, the fluorine spins are irradiated, and ^{1}H → ^{19}F-CP is thus generated. The use of double CP is to remove background signal in the ^{1}H channel. The evolutions of fluorine (during CP) and proton (in the CP-drain) magnetisation were observed as a function of contact time, t_{CP}, under high-resolution conditions with high-power ^{1}H and ^{19}F decoupling in the two experiments, respectively. The magnitude of the decoupling was about 75 kHz in this study. The spin–lattice relaxation times in the rotating frame for the ^{19}F ($T_{1\rho}^F$) and ^{1}H ($T_{1\rho}^H$) spins were measured by variable spin-lock time experiments. The relevant pulse sequences are depicted in Fig. 1d and e. In the $T_{1\rho}^F$ measurement, the initial ^{19}F magnetisation is generated by CP from ^{1}H with a short contact time (0.1 ms) and then spin-locked for a variable spin-lock time, t_{SL}. In the $T_{1\rho}^H$ measurement, the ^{1}H magnetisation is spin-locked for a variable t_{SL} and then transferred to ^{19}F by CP for 0.1 ms. The short contact time of 0.1 ms was used to enhance the magnetisation of fluorines closely attached to the spin-locked protons. As a further advantage, the dual channel CP approach suppresses any background signals from the probe in both ^{19}F and ^{1}H channels. The sequences also (except Fig. 1c) retain the advantage of the potentially greater resolution in the fluorine spectrum. The RF field strengths used for the spin-lock of ^{1}H and ^{19}F spins were kept at the same values as used for CP (i.e. equivalent to about 83 kHz). The free induction decays (FIDs) were acquired with high-power ^{1}H (or ^{19}F) decoupling.

The fast MAS experiments were carried out on a Bruker

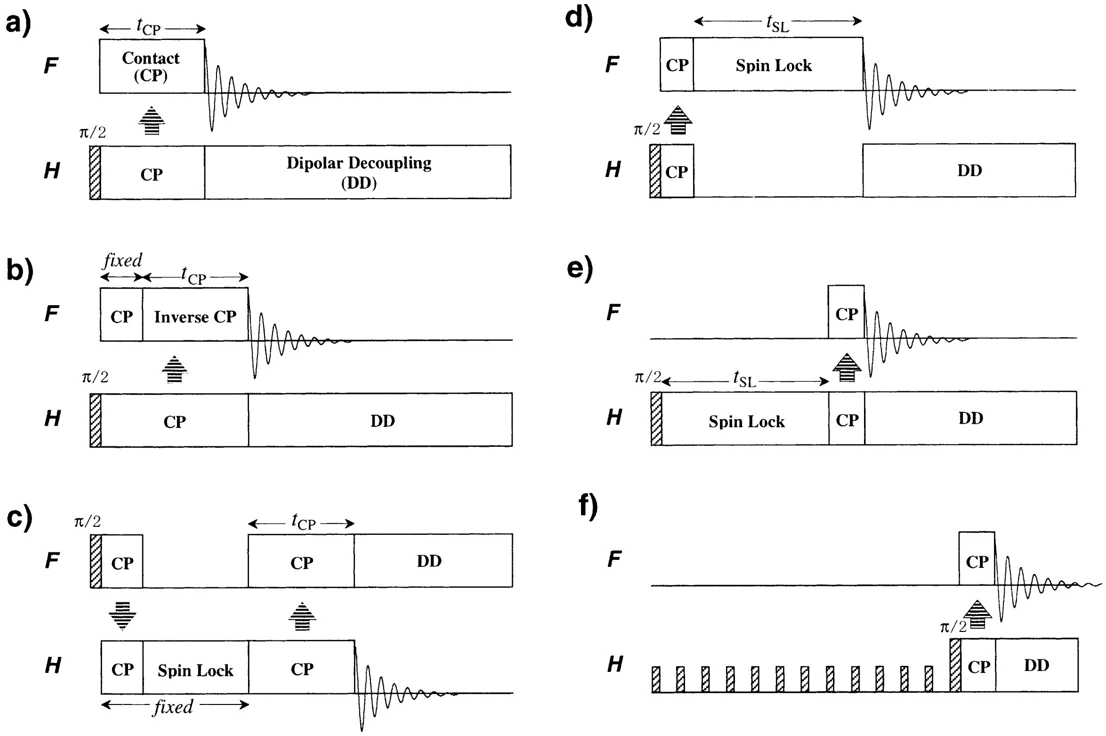

Fig. 1. Pulse sequences for (a) standard variable contact-time $^1H \rightarrow {}^{19}F$ CP, (b) variable contact-time $^1H \rightarrow {}^{19}F$ inversion recovery CP (IRCP), (c) variable contact-time CP-drain, (d) a short contact CP followed by a variable-time ^{19}F spin-lock, (e) a variable-time ^1H spin-lock followed by a short contact CP, and (f) selective observation of a region having a relatively long T_2^H (DIVAM) (see text in Sect. 3.4).

Avance DSX-300 spectrometer operating at a resonance frequency of 300.0 MHz for ^1H nuclei. A Bruker BL-2.5 MAS probe-head was used. The samples were spun using 2.5-mm o.d. zirconia rotors allowing for spinning frequencies of up to 35 kHz. The spectra were acquired using single-pulse excitation with a π/2 pulse duration of 3 μs, recycle delay of 5 s, spectral width of 125 kHz and 32 transients. Proton chemical shifts are quoted with respect to the signal for $Si(CH_3)_4$ (0.0 ppm) and were measured via replacement with a sample of 3-trimethylsilyl-1-propanesulfonic acid sodium salt (0.0 ppm).

Static pulsed NMR experiments for measuring T_2 were carried out on a Bruker minispec Mq-20 spectrometer operating at 20 MHz for ^1H nuclei. The signals were acquired using the solid-echo pulse sequence with a π/2 pulse duration of 2.5 μs, recycle delay of 10 s, and 256 transients. Static broad line NMR measurements were carried out on a Bruker MSL-100 spectrometer operating at 100 MHz for ^1H nuclei. A probe with extremely short ring-down time operating only at the proton frequency and with improved background response was used. Higher and lower temperature ^1H spectra were taken by using the temperature-control unit with a dried airflow. For the measurement of $T_{1\rho}^H$, the signals were acquired using the conventional spin-lock pulse sequence with a π/2 pulse duration of 2.0 μs, recycle delay of 10 s, and 128 transients. The RF field strength used for the spin-lock of ^1H spin was equivalent to about 100 kHz.

Solution-state ^{19}F-NMR measurements were carried out on a Varian Unity Inova-500 spectrometer operating at a resonance frequency of 470.3 MHz for ^{19}F nuclei at a temperature of 110°C. The $^{19}F-{}^1H$ *J*-coupling multiplicity was removed using the modulated WALTZ-16 decoupling sequence. The spectra were acquired using single-pulse excitation with a 30° pulse duration, recycle delay of 2 s, spectral width of 188 kHz and 32 transients. Fluorine chemical shifts are quoted with respect to the signal for $CFCl_3$ via replacement with a sample of liquid C_6F_6 (−164.3 ppm).

3. Results and discussion

3.1. Solution-state NMR

Fig. 2a shows a solution-state ^1H-decoupled ^{19}F-NMR spectrum of PVF dissolved in DMF-d_7. Bruch et al. have attempted to assign the solution-state ^{19}F spectrum of commercial PVF and of a sample synthesized in their laboratory using two-dimensional *J*-correlated experiments [17]. Their prediction of chemical shifts based on the rotational-isomeric-state (RIS) approximation [18] showed good agreement with their experimental data. Fig. 3 shows the variations in the chain microstructure (tacticity and regioregularity) of PVF in planar zig-zag projections, together with the assignments of the ^{19}F signals in our

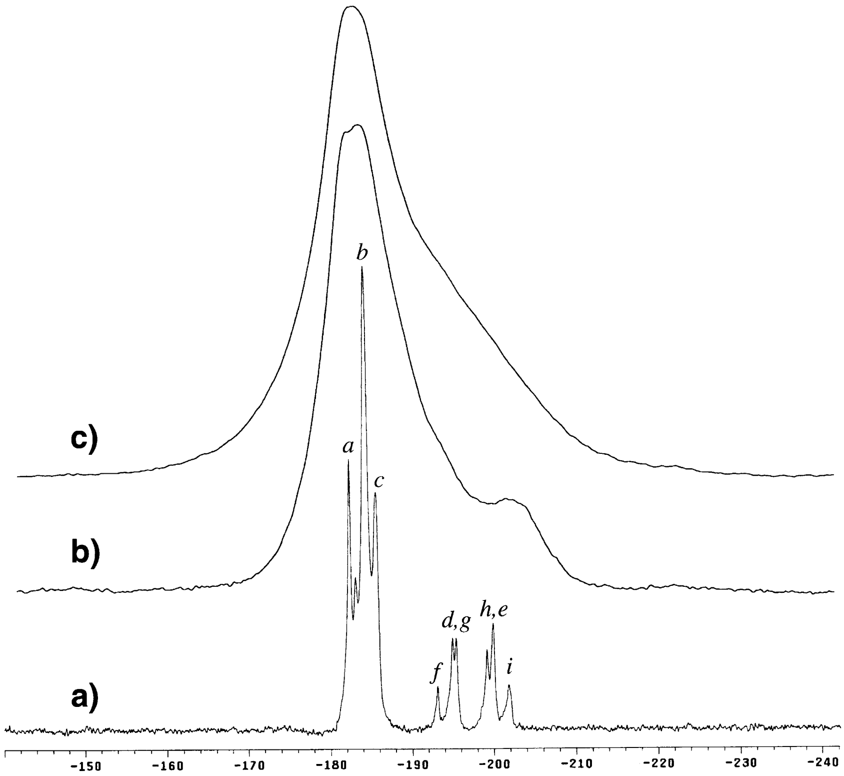

Fig. 2. ^{19}F-NMR spectra of poly(vinyl fluoride) (PVF): (a) proton-decoupled solution-state spectrum for a solution in DMF-d_7 measured at 110°C; solid-state direct polarisation MAS spectrum measured at 35°C (calibrated temperature) (b) with and (c) without ^{1}H decoupling at a spin rate of 13.5 kHz. The ^{1}H decoupling RF field during acquisition for (b) is equivalent to about 75 kHz.

solution-state spectrum. The *m* and *r* designate, as usual, the *meso* and *racemo* configurations between the fluorines in 1,3 positions, respectively. The underlined designations (*m*, *r*) represent the substituents in the regio-irregular 1,2 positions. The existence of HH linkages generates six split signals resonating at lower frequency by 7.4–18.7 ppm than those in regio-regular sequences (HT units). The fraction of the inverted units estimated from the integrated peak intensities of signals d and e against all the other peaks is ca. 11%, which is significantly higher than the defect percentages reported for PVDF (3–6%) [19].

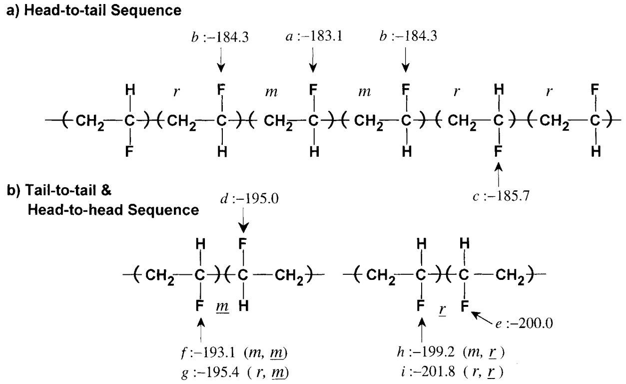

Fig. 3. The variations in the chain microstructure (tacticity and regioregularity) of PVF in a planar zig-zag projection and the assignments of the ^{19}F signals in the solution-state spectrum. The *italic* symbols and attached ^{19}F chemical shifts correspond to the peaks in the solution-state spectrum (Fig. 2a). The *m* and *r* designate the usual *meso* and *racemo* configurations between the fluorines in 1,3 positions, respectively. The underlined designations (*m*, *r*) represent the substituents in the regio-irregular 1,2 positions. The definitions of designations are same as those in Ref. [17].

3.2. Solid-state ^{19}F-MAS NMR

Fig. 2b and c shows the direct polarisation ^{19}F spectra of solid PVF powder, obtained at a spin rate of 13.5 kHz with and without high-power ^{1}H decoupling. The Bloch–Siegert effect, which is a chemical shift displacement of ca. 1.4 ppm caused by the ^{1}H decoupling, was corrected after the measurements (using standardised calibrations). Without the proton irradiation (Fig. 2c), the spectrum shows only an intense broad line around -183 ppm. This relatively featureless nature of the spectrum arises because of the significant dipolar interactions between fluorines and protons in PVF. On the other hand, the split signals resonated at -182 and -184 ppm and a shoulder at -202 ppm prominently appear in the decoupled spectra. It has been found that for heterogeneous polymers such as semicrystalline PVDF, new spectral features occur, which are caused by solid-state effects (e.g. different crystalline modifications). The new resonances observed for solid PVDF are not detectable in the solution state [4]. Although such new peaks are not observed in Fig. 2b, the comparison between the solid-state and solution-state spectra of PVF suggests that additional resonances may exist. Note that the chemical shifts of the bandshape near the maximum in the ^{1}H-decoupled MAS spectrum coincide well with those of peaks a and b in the solution spectrum (Figs. 2 and 3). This indicates that fluorines having similar electronic environments to those in solution may exist in the solid state.

3.3. ^{1}H pulsed NMR measurements

Although some of the spectral features become more pronounced in the ^{1}H-decoupled MAS spectrum, decomposition of the spectrum in Fig. 2b into immobile (crystalline) and mobile (amorphous) regions is not straightforward. In the case of PVDF, $T_{1\rho}^{\mathrm{H}}$ and $T_{1\rho}^{\mathrm{F}}$ of the crystalline region are about 4 times larger than those of the amorphous region, which facilitates the observation of the crystalline and the amorphous spectra selectively by long spin-locking and dipolar-dephasing experiments, respectively [3]. However, such experiments were not effective for PVF, as described below, due to the smaller difference in the relaxation times and significant spectral overlap between the immobile and mobile regions. Fig. 4a shows a $T_{1\rho}$ relaxation decay of the ^{1}H signal for the static state using the conventional spin-lock pulse sequence. Two single-exponential components are clearly seen, and the value of $T_{1\rho}^{\mathrm{H}}$ for the faster relaxing component (2.4 ms) is significantly shorter than that of the slower relaxing component (20 ms). The former and latter components are ascribed to the mobile and immobile regions of the polymer, and their proportions are estimated as 51 and 49%, respectively. Fig. 4b shows the T_2 relaxation decay of the ^{1}H signal for the static state using the solid-echo pulse sequence. Two single-exponential components were used to fit the decay curve (similar to the $T_{1\rho}$ situation), and the value of T_2^{H} for the faster relaxing component (5 μs) is much shorter than that of the slower relaxing component (130 μs). The former and the latter components are ascribed to the immobile and mobile region of the polymer, and their proportions are estimated as 93 and 7%, respectively. By utilising the difference in T_2^{H} between the two regions, we attempted to select the fluorine signal of mobile region (see below).

The static broad line ^{1}H-NMR spectra measured in the temperature range from 20 up to 130°C are shown in Fig. 5 together with their half-height-widths. The onset of the glass transition is estimated as ca. 40°C, which coincides well with the reported value (41°C). However, the temperature change of the linewidth as an indication of the glass transition occurs smoothly. The broad transition range should be an indication of a distribution of molecular mobilities in the immobile region. We have carried out some T_2^{H} and $T_{1\rho}^{\mathrm{H}}$ experiments below T_g. The linewidth changes with temperature also show that a remarkable percentage of the material is still mobile some ten degrees below the given T_g. Although the shape of the ^{1}H-NMR spectrum is not very differentiated even above T_g, there is a remarkable difference in the linewidths of the components (Fig. 5b). However, the transition between the immobile and mobile regions is hardly specifiable, which is in contrast to the situation for other polymers such as PVDF [20]. A superposition of more than three Gaussian and Lorentzian lines was necessary to deconvolute the spectrum measured at 130°C. The high degree of defects should be taken into account in order to explain the temperature behaviour. Similarly, the environment of the defects could cause relatively slow molecular motions, which are responsible for the $T_{1\rho}$ relaxation, whereas the T_2 relaxation is sensitive to even lower frequencies than $T_{1\rho}$. Hence, different populations of the mobile and the immobile regions obtained from $T_{1\rho}$ and T_2 relaxation data are not contradictory. Furthermore, there is an additional influence of the relaxation in the rotating frame on the line shape of the immobile region. The linewidth becomes broader with increasing spin-locking times (spectra are not shown), which indicates that the region with the long $T_{1\rho}^{\mathrm{H}}$ (immobile region) has the shorter T_2^{H}. In

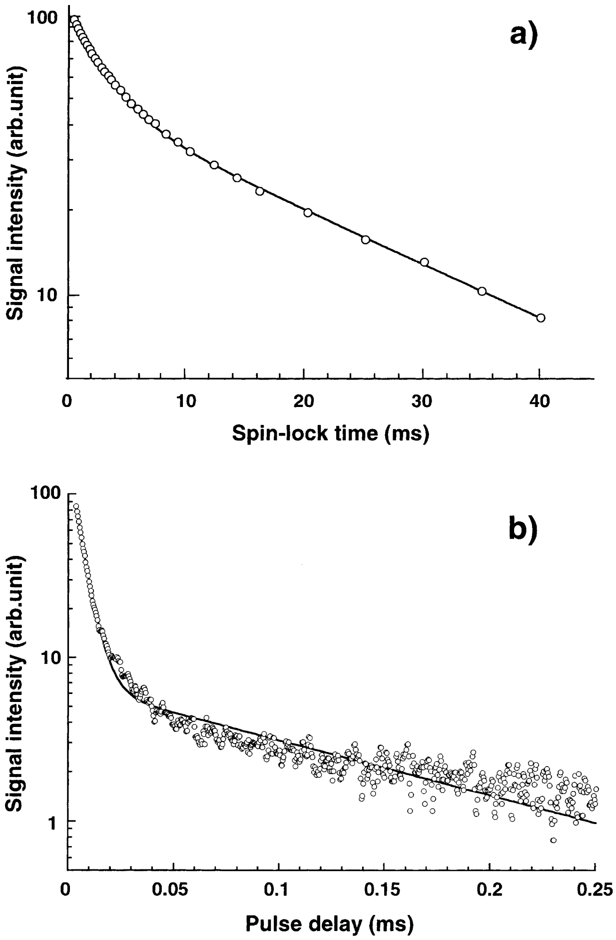

Fig. 4. (a) $T_{1\rho}$ relaxation plot for the ^{1}H signal of PVF in the static state obtained by using the spin-lock pulse sequence, and (b) T_2 relaxation plot for the ^{1}H signal of PVF in the static state obtained by using the solid-echo pulse sequence. Both experiments were carried out at ambient probe temperature (22°C), and both decays were fitted by double-exponential functions.

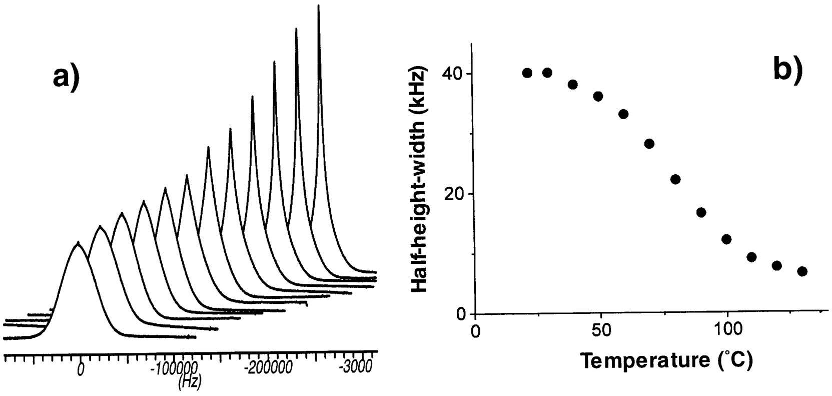

Fig. 5. Static ^{1}H broad line NMR spectra measured from 22 to 130°C at 10°C intervals (from bottom to top), and the dependence of the linewidth (full width in half height) on the temperature.

contrast, the line shape remains unchanged for long spin-locking times in PVDF [20].

Spin-diffusion is a very useful technique to obtain information about the extent and the nature of heterogeneities in polymers. Therefore, it has been attempted to carry out static ^{1}H-NMR experiments using the Goldman–Shen type phase selection [21,22], which are commonly in use for heterogeneous polymers, at two temperatures. For the first experiment, a temperature of 22°C was chosen because a remarkable mobility of a small part of PVF was still present below T_g. However, the superimposed effect of the longitudinal relaxation in combination with the small population of the residual mobile component disables the numerical exploitation of the effect. In the proximity of T_g, the relatively short T_1^H complicates the application of spin-diffusion techniques. The longitudinal relaxation was proved to be a single exponential. Furthermore, it seems hard to create a clear phase separation between the mobile and immobile regions by the Goldman–Shen method at 22°C. Possibly, there is a broader distribution of domain sizes and mobility properties as well, which must be taken into account.

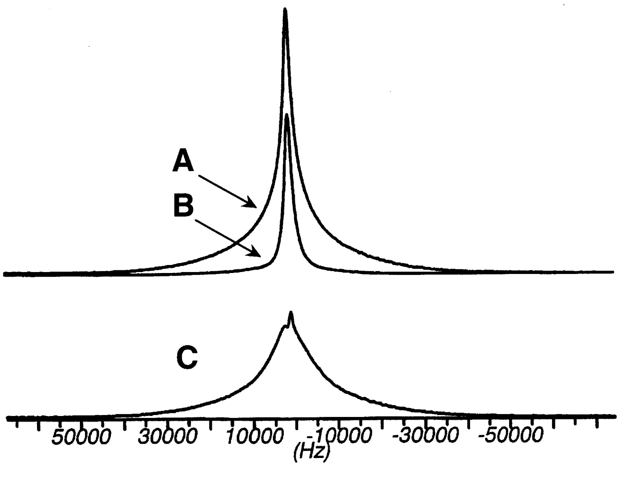

Fig. 6. (A) Static ^{1}H broad line spectrum measured at 130°C, (B) the narrow component obtained after a post-pulse pre-acquisition delay time of 100 μs, and (C) the broad component generated by subtraction of (B) from (A). The narrow and broad components have linewidths of 2.5 and 14.8 kHz, respectively. The lineshape of the narrow component was used for the selection of the mobile region in the spin-diffusion experiment.

As shown in Fig. 6, the residual experimental line shape after a post-pulse pre-acquisition delay (without spin-locking) of 100 μs (spectrum B) can be taken as a representative of the mobile region. Both spectra A and B of Fig. 6 were observed at 130°C. The subtraction of the spectrum of the mobile region from the complete spectrum yields the spectrum of the immobile region of PVF (spectrum C). This temperature, being ca. 90 K above T_g, has been chosen because the population of the mobile and immobile regions of PVF are of comparable order. The spin-diffusion experiment has been repeated at 130°C as shown in Fig. 7. Furthermore, the influence of the longitudinal relaxation is smaller at this temperature due to the longer T_1^H, and the spin-diffusion effect can be separated much better by the greater difference in the molecular mobilities. Although numerical separation of the lineshapes is more complicated at higher temperatures, due to the distribution of molecular mobility and domain sizes, spectrum C in Fig. 6 can be taken to represent the immobile region. An arbitrary two-phase structure was assumed for PVF with volume fractions of the rigid and the mobile components which can approximately be obtained as the ratio of the broad and narrow lines in the static ^{1}H spectrum. On the other hand, we assumed that the remaining signal after the selection phase can be taken as the line shape function of the mobile region as described above. The complication to define a starting magnetisation could be concerned with the deconvolution of the line shape. The intensity does not start at zero at $t_{\mathrm{mix}} = 0$, since the difference in T_2 is not completely selective. The calculated line shape of the broad part should be identical for all mixing times t_{mix}, if this assumption is correct. To assume reliable values for the spin-diffusion coefficients (D), these values should be proportional to the dipolar interaction (half-height-width) taken from the spectra of the mobile

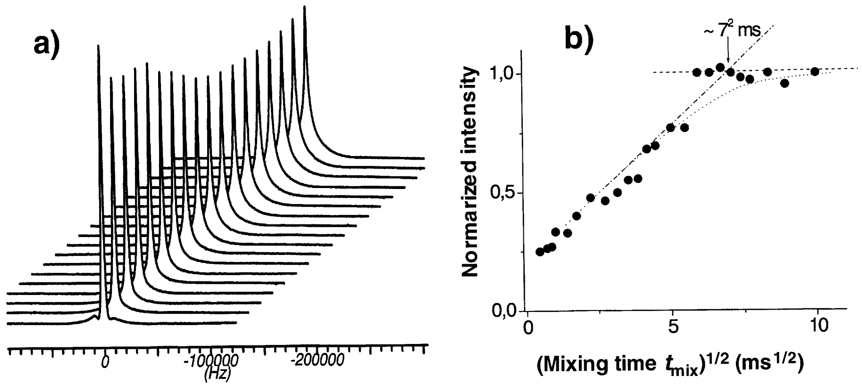

Fig. 7. (a) Static ^{1}H broad line spectra after a Goldman–Shen pulse sequence (the mixing times increase from bottom to top according to the data on the right side) and (b) the recovery function of the magnetisation of the immobile region in a spin-diffusion experiment carried out at 130°C.

and immobile regions according to the technique described below. The narrow half-height-width is about 2.4 kHz and the broader one about 14.8 kHz. An effective spin-diffusion coefficient (D_{eff}) using the approach described in Ref. [22] has been obtained from Eq. (1):

$$\sqrt{D_{\mathrm{eff}}} = \frac{2\sqrt{D_{\mathrm{m}}D_{\mathrm{i}}}}{(\sqrt{D_{\mathrm{m}}} + \sqrt{D_{\mathrm{i}}})} \tag{1}$$

where D_{m} and D_{i} are the intrinsic spin-diffusion coefficients of the mobile and immobile regions, respectively. The linewidths of the narrow and the broad components are in a ratio of 1:6. For the data treatment, it should be reasonable to assume that the spin-diffusion coefficients have also the same relation of 1:6 ($D_{\mathrm{m}}/D_{\mathrm{i}}$). The value of D_{m} has been taken as 0.05 mm^{2} s^{-1} for the mobile phase, and that of D_{i} for the broader component as 0.30 mm^{2} s^{-1} by relation to data given in the literature for semicrystalline polymers [22]. These values have been scaled with the reduced linewidths at higher temperature, which gives an average D_{eff} of 0.1 mm^{2} s^{-1}. The characteristic spin-diffusion time of the immobile region $t_{\mathrm{s}}^{\mathrm{i}}$ has been taken from the intersection of the initial slope of the recovery function with the saturation value of the exchange process. In the crystallites of PVF, there is a mirror-plane perpendicular to both the *a*- and *c*-axes, and an extended planar zig-zag conformation is derived from the *c*-spacing. This crystalline structure is suitable to form lamellae like polyethylene or PVDF. If we assume a lamellar structure for PVF, a one-dimensional model can be applied to get a measure for the extent of the heterogeneities. A measure of the domain size has been taken using

$$d_{\mathrm{i}} = \frac{\varepsilon}{\chi_{\mathrm{i}}}\sqrt{\frac{4}{\pi}D_{\mathrm{eff}}t_{\mathrm{s}}^{\mathrm{i}}} \tag{2}$$

where ε denotes a parameter describing the dimensionality of the spin-diffusion process, which is equal to 1 in case of the lamellar structure [22]. The parameter χ_i that describes the population of the immobile component has been taken as 0.6 from the population of the immobile region at 130°C (Fig. 6). This value coincides with the crystallinity of PVF (60%) determined from X-ray diffraction data [13]. With a spin-diffusion time $t_{\mathrm{s}}^{\mathrm{i}}$ of about 49 ms and using this value, the estimation of a measure for the lamellar size yields about 4.2 nm.

3.4. $^{1}H \rightarrow$ ^{19}F-CP-MAS measurements

Fig. 1f shows a newly developed pulse sequence that can selectively observe signals having long T_2^{H}. A series of weak and short (3 μs) pulses with the same phase are applied to the ^{1}H channel with 20 μs intervals. During the minipulses, ^{1}H magnetisations from both immobile and mobile regions precess about B_1 with a pulse angle that depends on the pulse power. Between minipulses, the residual *z*-components of magnetisation are retained (pulse interval $\ll T_1^{\mathrm{H}}$ values) while the *y*-components partially relax (to different extents since T_2^{H} for the rigid regions is significantly less than that for the amorphous domains). This process reduces both the magnitudes of the two magnetisations and their pulse angles. The extent of these reductions depends on the pulse angle at the end of any given minipulse. The total pulse angle accumulated at the end of the series of minipulses is clearly a function of the minipulse power. It is evident that this angle (and the residual magnetisation magnitude) for the crystalline domains will be substantially less than that of the amorphous domains, provided the minipulse interval lies between the two relevant values of T_2^{H}. In this way, substantial discrimination between the domains can be built up. We call this new pulse technique 'discrimination induced by variable amplitude minipulses' (DIVAM). Any off-resonance effects are ignored in the above discussion. We are currently carrying out a more rigorous evaluation of this pulse sequence and its variants. After the pulse train, *y*-magnetisation is generated by applying a 90° pulse, and this is then spin-locked and cross-polarised to the ^{19}F spins. Fig. 8 shows the observed ^{19}F-CP-MAS spectra, using the DIVAM pulse sequence, with variation in the power of the weak pulses. When the power

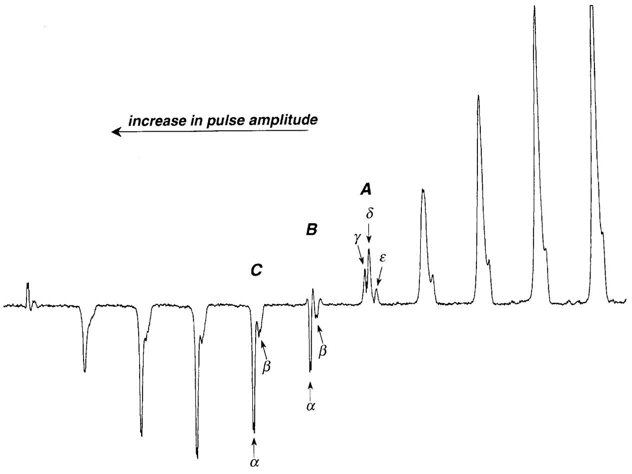

Fig. 8. The variations in the ^{19}F-CP-MAS spectra observed using the DIVAM pulse sequence shown in Fig. 1f as a function of the power of the minipulses. The series of minipulses of a 3 μs duration with the same phase are applied to the ^{1}H channel with 17 μs intervals. When the power is gradually increased (from the right to the left), the narrow peaks depicted by α and β were selectively inverted, while the three peaks depicted by γ, δ, and ε were not effectively inverted but decreased in intensity.

was gradually increased (from right to left), the narrow peaks depicted by α and β were selectively inverted, while the three peaks, depicted by γ, δ, and ε, were not effectively inverted until significantly higher powers were used. The peak splittings are clearly seen for α and β in spectrum B. The ^{19}F-CP-MAS spectra measured by this pulse sequence with intermediate powers can be understood as a superposition of effectively inverted signals having two peaks with splittings and the ineffectively inverted signals having three peaks. Since the ineffectively inverted signals relax to almost zero in spectrum C, the effectively inverted signals are selectively observed. Spectrum C, which consists of signals α and β, can be fitted by a combination of four Lorentzian functions as shown in Fig. 9. Note that the spectral lineshape and the chemical shifts of each component (−181.5, −184.2, −193.8, −198.9 ppm) are similar to those of the solution-state spectrum (Fig. 2a). As has been reported for PVDF, the amorphous region in the solid state resonates at similar positions to those in the solution-state spectrum [3,4]. Hence, we can assume that the effectively inverted signals may be assigned to the mobile region of PVF. The effective molecular motion in the mobile region averages the inherent chemical shifts of fluorines originating from the variations in conformation and intermolecular packing in the solid state, and thus the spectrum of the mobile region of the solid shows similarity to the solution-state spectrum. Accordingly, the signal resonating at −181.5 ppm in Fig. 9 is assigned to *mm*-units, and that at −184.2 ppm is assigned to overlapping *mr*- and *rr*-units. The other two signals resonating at the lower frequencies are assigned to fluorines adjacent to regio-irregular HH

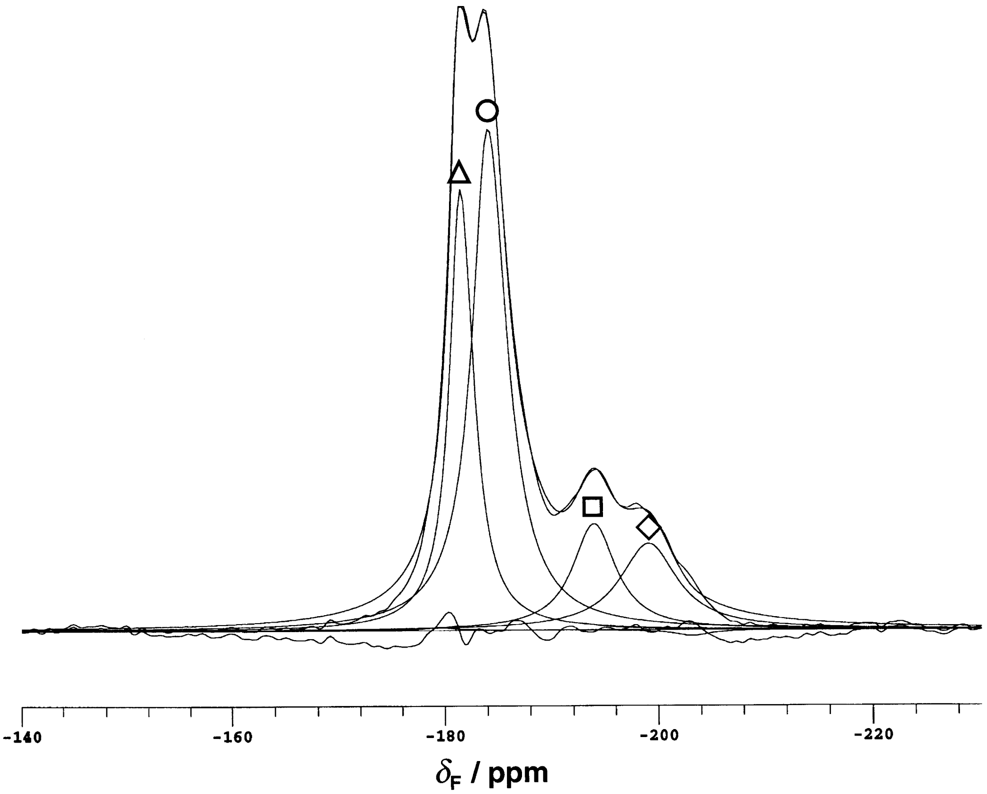

Fig. 9. ^{19}F-CP-MAS spectra of the effectively inverted signals (spectrum C in Fig. 8) obtained by using the DIVAM pulse sequence. This spectrum can be fitted by a combination of four Lorentzian functions.

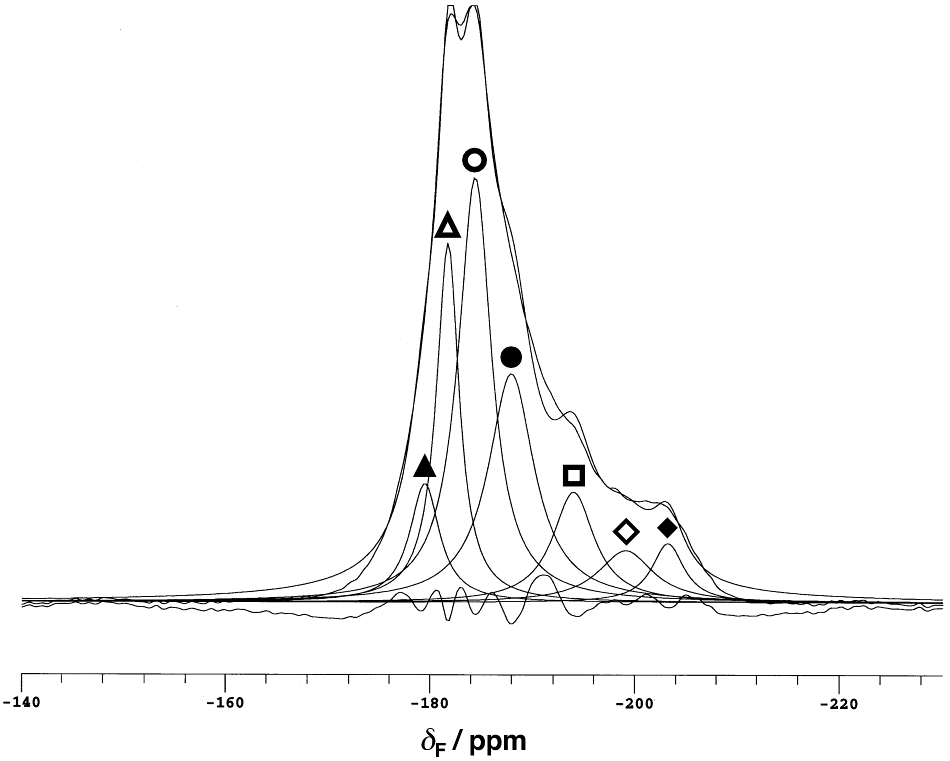

Fig. 10. Solid-state ^{1}H → ^{19}F-CP-MAS spectrum of PVF at a contact time $t_{CP} = 0.3$ ms. The spectral decomposition using seven Lorentzian functions is also shown. The peaks with open symbols have the same chemical shifts and half-height-widths as those in Fig. 9. The three residual signals with filled symbols are also fitted by Lorentzian functions.

linkages, as have been observed in the solution-state spectrum [17,18].

The ineffectively inverted signals shown in Fig. 8 may be detected by subtracting the effectively inverted signals (Fig. 9) from a conventional ^{1}H → ^{19}F CP/MAS spectrum with ^{1}H decoupling shown in Fig. 10. Spectral decomposition using seven Lorentzian functions is also shown in the figure, in which the signals with open symbols have the same chemical shifts and half-height-widths as those in Fig. 9. This indicates that the residual (ineffectively inverted) signals (γ, δ, and ε) can be fitted by three Lorentzian functions (shown with filled symbols). These can be assigned to the immobile regions in PVF. No such peaks are found in the solution-state spectrum, which is consistent with the PVDF case [3,4]. The chemical shifts of the seven signals are summarised in Table 1, and no significant difference is observed in the half-height-widths between the mobile and immobile regions. The integral of immobile signals (36%) is smaller than that of the mobile signals (64%) in Fig. 10. Since the former value is smaller than the proportion of the immobile region determined from the static broad line ^{1}H-NMR spectra measured at 130°C (60%), the half-height-widths of the immobile signals might be underestimated. However, the variations of peak heights in the spin-lock, standard CP, and inversion recovery CP experiments clearly exhibit the characteristics of the immobile region as described below.

In the case of PVDF, the spectral difference between the α and β crystalline forms was explained on the basis of chain conformation, taking into account the γ-*gauche* shielding effect [4]. However, the signals for the immobile regions in PVF are not readily ascribed to such a variation in the crystalline forms because only the planar zig-zag conformation has been reported for PVF. As has been revealed by Li and Chesnut [23], repulsive van der Waals interactions are associated with deshielding effects in observed chemical shifts. Grover et al. demonstrated that the *syn*-axial orientation of neighbouring δ-nuclei in methylnorbornane, methyldecalin, and pregnane produces appreciable deshielding shifts (δ-effect), as large as 5 ppm [24]. Fig. 11 shows a

Table 1
The spin–lattice relaxation in the rotating frame and the cross polarization parameters of each spectral component in Fig. 10 of PVF determined from the variable spin-lock time and the variable contact time experiments (unit: ms)

Chemical shift (ppm)	$T_{1\rho}^{F}$	$T_{1\rho}^{H}$	T_{HF}^{*}	$T_{1\rho}^{*}$	Nature
▲−179.3	21.8	14.9	0.04	11.1	Immobile
△−181.5	14.4	8.2	0.08	8.9	Mobile
○−184.2	13.9	8.6	0.07	9.2	Mobile
●−187.8	25.8	14.1	0.04	12.0	Immobile
□−193.8	15.2	9.4	0.07	10.1	Mobile
◇−198.9	10.9	6.8	0.07	9.2	Mobile
◆−203.1	33.0	14.7	0.04	13.5	Immobile

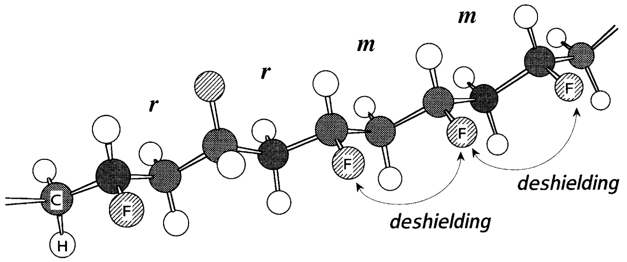

Fig. 11. Schematic view of a PVF polymer chain having a planar zig-zag conformation. When two fluorines are located in a *meso*-position, they are mutually deshielded by the δ-effect. Fluorines located in the *mm*-dyad units are doubly deshielded, and those in the *mr*-units are singly deshielded.

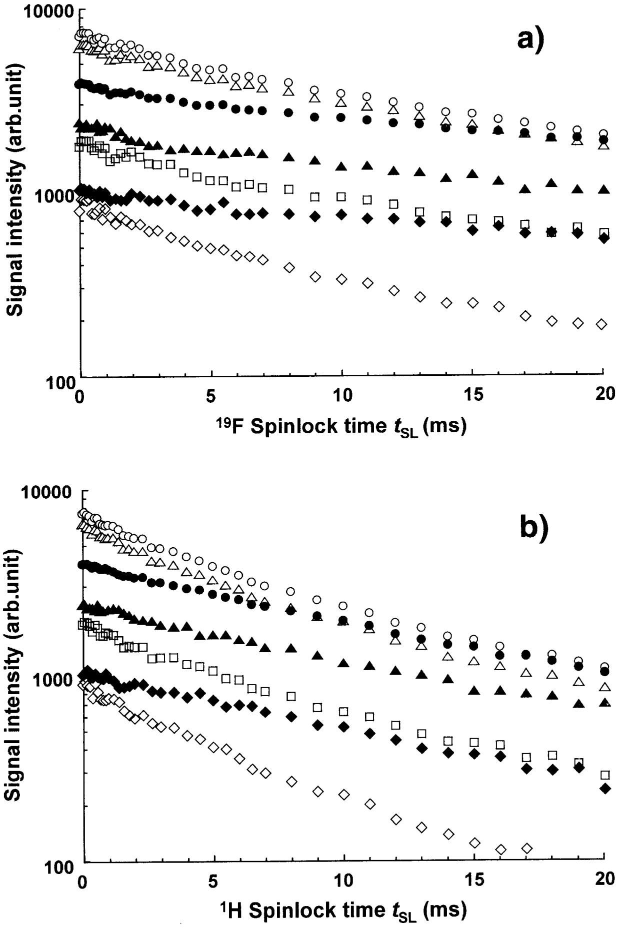

Fig. 12. Spin-lock-time dependence of the ^{19}F signal intensity for PVF for (a) ^{1}H → ^{19}F CP followed by ^{19}F spin-lock, and (b) ^{1}H spin-lock followed by ^{1}H → ^{19}F CP. The open and filled symbols correspond to the peaks in Fig. 10. The directly measured $T_{1\rho}^{F}$ and indirectly measured $T_{1\rho}^{F}$ obtained using single-exponential functions are summarised in Table 1.

schematic view of a PVF polymer chain having a planar zig-zag conformation. Since the two fluorines located in a *meso*-position take a *syn*-axial orientation, they should be mutually deshielded by the δ-effect. Accordingly, the fluorines located in the *mm*-dyad units are doubly deshielded, and those in the *mr*-units are singly deshielded. Hence, the signals resonating at −179.3 and −187.8 ppm are tentatively assigned to fluorines of the *mm*-units and *mr*-units in the immobile region, respectively. The fluorines of the *rr*-units should exhibit signals overlapping with the mobile signal resonating at −193.8 ppm, so they are not separately observed. In the spectra of the crystalline phases of PVDF, the fluorine signals at HH-linkages are almost lost, and it was concluded that the regio-irregular units predominantly exist in the mobile region [3,4]. However, we assigned the signal resonating at the lowest frequency (−203.1 ppm) in Fig. 10 to fluorines existing at HH-linkages in PVF because a significant amount of such linkages is included in the crystalline region of PVF [14], and their content is much higher than that of PVDF.

The decays of ^{19}F magnetisation observed in the ^{1}H → ^{19}F CP followed by the variable ^{19}F spin-lock experiment are shown in Fig. 12a as a function of the spin-lock time, t_{SL}. A series of spectra with varying t_{SL} were decomposed into seven Lorentzian functions whose chemical shifts and half-height-widths were fixed to those derived from Fig. 10. The open and filled symbols used in Fig. 12 correspond to those in Fig. 10. The decays of ^{19}F magnetisation observed in the experiment with variable ^{1}H spin-lock time followed by ^{1}H → ^{19}F CP are shown in Fig. 12b in the same manner as for Fig. 12a. The directly measured $T_{1\rho}^{F}$ and the indirectly measured $T_{1\rho}^{H}$ (via ^{19}F resonance) data thus obtained using single exponential functions are summarised in Table 1. All the curves of the immobile regions (filled symbols) in Fig. 12a and b were well fitted by single exponential functions, while the curves of the mobile regions (open symbols) have significant contributions from short $T_{1\rho}^{F}$ and $T_{1\rho}^{H}$ components. This suggests that the values of $T_{1\rho}^{F}$ and $T_{1\rho}^{H}$ of the mobile region may be smaller than those determined from the slope of the relaxation curves derived from ^{1}H spin-lock experiments in the static state. It was not easy to apply double exponential fitting to the relaxation decays of the mobile regions due to the small difference between the short and the long relaxation times. However, the average values of $T_{1\rho}^{F}$ and $T_{1\rho}^{H}$ of the immobile regions determined by single exponentials (26.9 and 14.6 ms) are significantly larger than those of the mobile regions (13.6 and 8.3 ms). Homo-nuclear spin-diffusion promoted by the spectral overlap should occur to some extent between the two regions (depending on the domain sizes), and this effect will tend to average the $T_{1\rho}^{F}$ and $T_{1\rho}^{H}$ values. Note that the differences in the $T_{1\rho}$s determined by single exponentials between the immobile and mobile regions are much smaller than in the case of PVDF, for which the $T_{1\rho}^{F}$ of the immobile region is ca. 3.5 times larger than that of the mobile region, and no significant spin-diffusion effects were observed in the spin-lock experiments [3]. These findings lead us to two possible conclusions: one is that the difference in mobility between the two regions in PVF is much smaller than that for PVDF. This is supported by the irregularity in the crystalline structure of PVF. The other is that the crystalline and amorphous domain sizes of PVF are much smaller than in PVDF, so that somewhat more effective spin-diffusion occurs between the two regions in the former.

The evolutions of the ^{19}F magnetisation obtained from the standard $^{1}\mathrm{H} \rightarrow {}^{19}\mathrm{F}$ CP experiments are shown in Fig. 13a as functions of the contact time, t_{CP}. All the CP curves can be well fitted by a double-exponential function

$$M(t) = A\left\{-\exp\left(-\frac{t_{\mathrm{CP}}}{T_{\mathrm{HF}}^{*}}\right) + \exp\left(-\frac{t_{\mathrm{CP}}}{T_{1\rho}^{*}}\right)\right\}, \tag{3}$$

where T_{HF}^{*} and $T_{1\rho}^{*}$ are effective parameters that characterise the increase and decrease of fluorine magnetisation (the HF in T_{HF}^{*} indicates that the polarisation is transferred from proton to fluorine), while A is a fitting parameter for the signal intensity. This indicates that the increase and the decrease of magnetisation can be expressed by single-exponential behaviour. The effective time constants determined from the fitting of the experimental curves, T_{HF}^{*} and $T_{1\rho}^{*}$, are given in Table 1. Since the ratio of the number of F spins to the H spins is not small (33 at.%) and the $T_{1\rho}^{\mathrm{H}}$ and $T_{1\rho}^{\mathrm{F}}$ relaxation processes are comparable in efficiency, there is no simple method to infer the true values of T_{HF} and $T_{1\rho}^{\mathrm{H}}$ from the T_{HF}^{*} and $T_{1\rho}^{*}$. However, the peaks of the immobile region show significantly shorter T_{HF}^{*} and longer $T_{1\rho}^{*}$ than those of the mobile region. The short T_{HF}^{*} indicates that cross polarisation occurs more effectively in the immobile region due to the strong hetero-nuclear dipolar interactions. Moreover, the long $T_{1\rho}^{*}$ is also indicative of strong dipolar interactions.

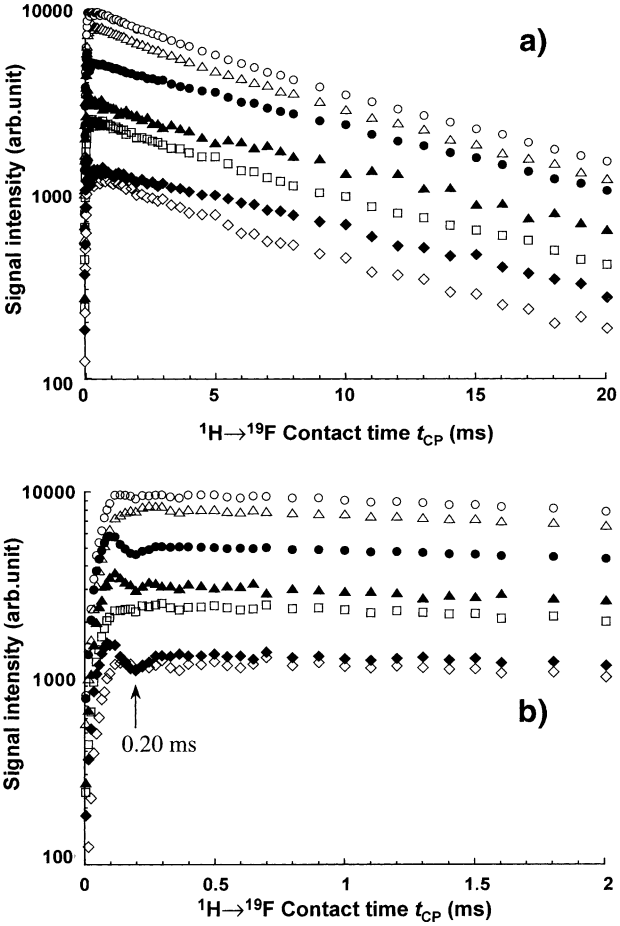

Fig. 13. (a) Contact-time dependence of the ^{19}F signal intensity for the $^{1}\mathrm{H} \rightarrow {}^{19}\mathrm{F}$ CP experiment on PVF, and (b) its magnification for short contact times to show the dipolar oscillation behaviour. These oscillations are observed only for the signals originating from the immobile region. The oscillation frequency is estimated as 5 kHz.

Since the polarisation transfer inherently includes a coherent process, a two-stage feature is frequently detected in the initial period of cross polarisation, when there is a strongly coupled H–X spin pair [25,26]. The first stage originates from coherent energy transfer between directly bonded H and X spins, causing dipolar oscillation. In the second stage, an equilibration of magnetisation occurs within the H spin bath via homo-nuclear spin-diffusion. As clearly seen in the magnification of the initial stage of $^{1}\mathrm{H} \rightarrow {}^{19}\mathrm{F}$ CP (Fig. 13b), the dipolar oscillations are observed for the immobile region. This fact indicates that there is a strongly coupled H–F spin pair in the immobile region but that the hetero-nuclear dipolar interactions are substantially reduced in the mobile region by motional averaging. We have analyzed the transient oscillations observed in the $^{1}\mathrm{H} \rightarrow {}^{13}\mathrm{C}$ CP curves of poly(trifluoroethylene) (PTrFE) in order to determine the effective bond distances [27]. The dipolar oscillation frequency, f_{osc} (Hz), can be expressed as

$$f_{\mathrm{osc}} = \frac{\mu_0 \gamma_{\mathrm{H}} \gamma_{\mathrm{F}} \hbar}{16\sqrt{2}\pi^2 r_{\mathrm{HF}}^3} \tag{4}$$

where γ_{F} and γ_{H} are the gyromagnetic ratios, and r_{HF} is the interatomic distance between hydrogen and fluorine [25,28]. The first peaks and dips for PVF are observed at 0.10 and 0.20 ms, respectively, for all the CP curves of the immobile regions, which corresponds to $f_{\mathrm{osc}} = 5$ kHz. The distance r_{HF} thus calculated using the above equation is 2.0 Å. This value coincides well with a calculated H···F distance for the H–C–F group (2.02 Å) of a tetramer model of PVF.[2] It is surprising that this agreement of the H···F distances indicates there is no effective motional averaging of the hetero-nuclear dipolar interactions in the immobile region of PVF at ambient probe temperature despite the imperfection of the crystalline structure. The effective average C–H bond distance in PTrFE calculated from dipolar oscillations at ambient probe temperature was 1.5 Å, which is significantly longer than the expected rigid lattice value (1.1 Å). The difference of the bond distances was ascribed to motion of the polymer chain. The above results indicate that such molecular motion (in the order of several tens of kHz) may exist only in the mobile region for PVF. The evolutions

---

[2] A density functional level of theory (B3LYP) with an extended basis set with polarization functions (6-31G(d,p)), which is implemented in the 'GAUSSIAN-98' (Revision A.7) program, were used for the geometry optimization.

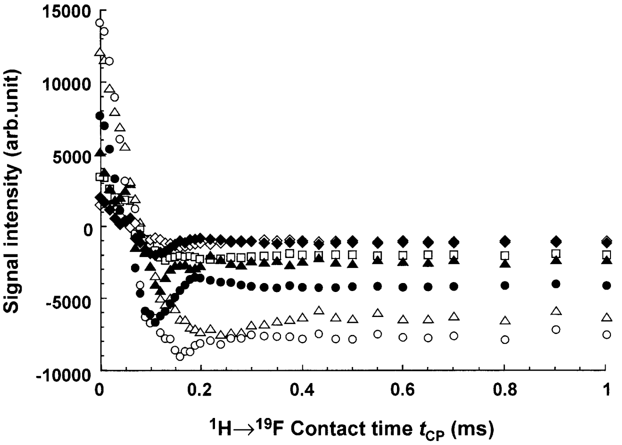

Fig. 14. Contact-time dependence of the ^{19}F signal intensity for the $^1H \rightarrow ^{19}F$ inversion recovery CP (IRCP) experiment on PVF. Dipolar oscillation behaviours are observed not only for the immobile region but also for the mobile region. The dips of the dipolar oscillation for the mobile region are observed at longer contact times than those of the immobile region.

of ^{19}F magnetisations obtained from the $^1H \rightarrow ^{19}F$ IRCP experiments are shown in Fig. 14. Although there is no difference in the spin dynamics between the CP and IRCP experiments, IRCP is superior to the standard CP in observing details of CP processes. The dipolar oscillations are clearly observed in the initial stage not only for the immobile regions, but also for the mobile regions. The first dips observed for the immobile signals are at 0.10–0.12 ms, whereas those for the mobile signals resonating at −181.5 and −184.4 ppm are at 0.16 and around 0.22 ms, respectively. The effective average F–H bond distances calculated from these values are 2.3 and 2.6 Å, which are significantly longer than the expected rigid lattice value (2.0 Å) as described above. This difference is straightforwardly ascribed to motion of the polymer chain in the mobile region. As has been stated, the IRCP experiment is superior to the standard CP for observing the dipolar oscillation behaviours.

3.5. $^{19}F \rightarrow ^1H$ CP-MAS and ^1H MAS measurements

Fig. 15 shows the $^{19}F \rightarrow ^1H$ CP-MAS spectrum of PVF with ^{19}F decoupling. The spinning side bands originate from the residual dipolar interactions that are not averaged out by MAS at a spin rate of 13.5 kHz. Since a distinct shoulder is seen on the lower frequency side of the main peak (see the magnified spectrum), the line shape cannot be fitted by a single Lorentzian function. In addition, the half-height width of 1750 Hz is considerably larger than that of the ^1H MAS spectrum of a fluorinated polyimide (1100 Hz) whose single peak was well fitted by a single Lorentzian function [11]. In order to examine the origin of this shoulder, fast MAS measurements were performed to average the residual homo-nuclear dipolar interactions. Fig. 16

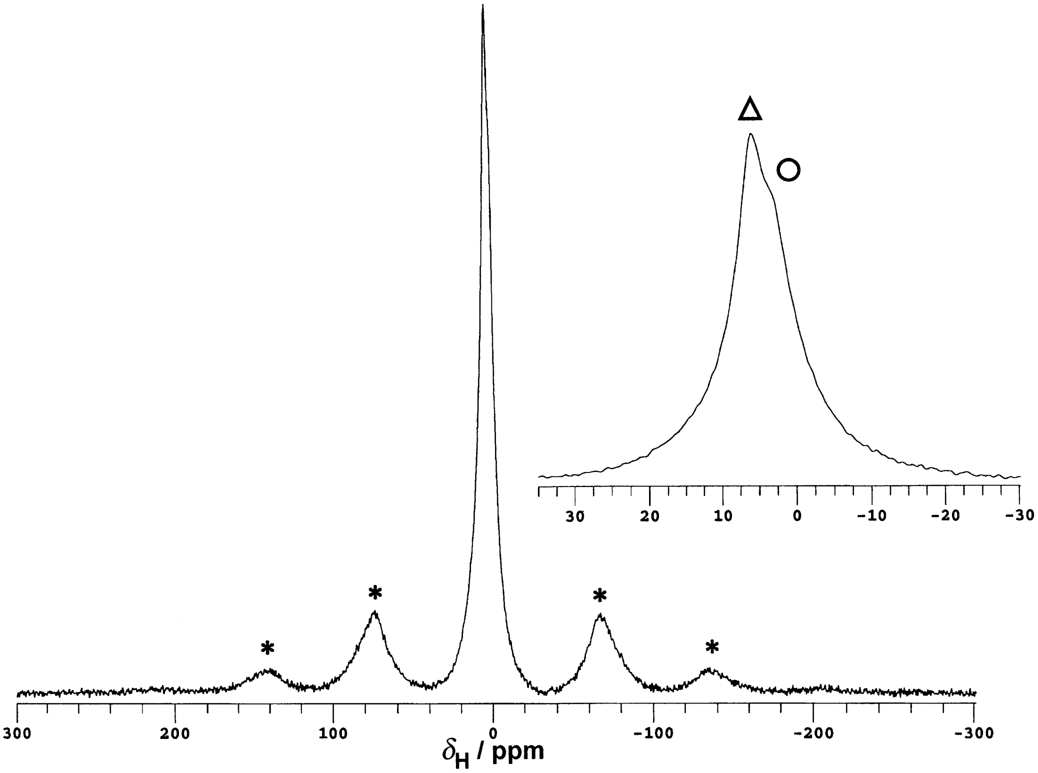

Fig. 15. Solid-state $^{19}F \rightarrow ^1H$ CP-MAS spectrum of PVF and the magnification of the main peak. A distinct shoulder is seen on the low-frequency side of the main peak. The spinning sidebands (marked by asterisks) that originate from the residual dipolar interaction are not averaged out by MAS at the spin rate of 13.5 kHz.

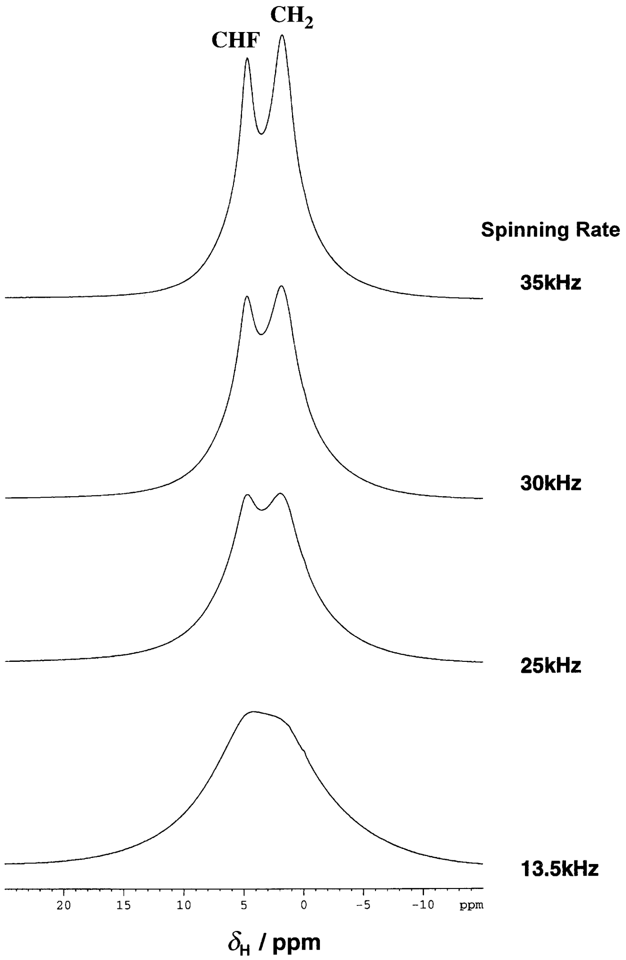

Fig. 16. Solid-state ^1H fast MAS spectra of PVF at spin rates of 13.5–35 kHz without ^{19}F decoupling. The line shape at 35 kHz is well fitted by two Lorentzian functions.

shows ^1H MAS spectra of PVF without ^{19}F decoupling measured at spin rates of 13.5–35 kHz. Despite the absence of ^{19}F decoupling, a shoulder can be observed on the lower frequency side in the ^1H MAS spectra at 13.5 kHz (the same spin rate as for $^{19}F \rightarrow {}^1H$ CP-MAS). As the spin rate is increased from 13.5 to 35 kHz, the main signal gradually splits into two peaks, and the lineshape is well fitted by two Lorentzian functions at 35 kHz. The chemical shifts of the peaks at higher and lower frequencies are 4.75 and 1.85 ppm referenced to TMS. The ratio of the integrated intensities is 0.38:0.62. Since the chemical shifts of the CHF and CH_2 protons of PVF swollen in Me_2SO-d_6 were reported as 4.8 and 2.0 ppm, respectively [29], the two peaks in the ^1H MAS spectra are straightforwardly assigned to the CHF and CH_2 protons. Note that the CHF protons, which have only half the magnetisation of the CH_2 protons, exhibit an apparently larger contribution to the peak maximum in the spectrum at 13.5 kHz. This is because the CHF proton signal has a narrower linewidth than the CH_2 proton signal. The hetero-nuclear (H–F) and homo-nuclear (H–H) dipolar interactions at CHF protons are effectively averaged by dipolar decoupling and spinning at 13.5 kHz, whereas the homo-nuclear dipolar interactions between two protons in the CH_2 groups are not averaged at this spin rate.

Although the signals of the CHF and CH_2 protons are appreciably overlapping in the $^{19}F \rightarrow {}^1H$ CP spectrum (Fig. 15), the contributions of these protons were tentatively estimated by fitting the spectrum using two Lorentzian functions, with peaks at 5.9 and 2.1 ppm. Fig. 17 shows the evolution of the peak heights of the two functions as a function of t_{CP} ($^{19}F \rightarrow {}^1H$ CP curves). The symbols in the figure correspond to those in Fig. 15. An influence of the dipolar oscillation inducing a maximum peak at 0.15 ms is observed for the CHF protons, whereas no such maximum is observed for the CH_2 protons. This is because the ^{19}F magnetisation rapidly transfers to the protons in the same CHF group, but homo-nuclear spin diffusion and/or long-distance CP from the fluorines at the adjacent CHF groups are necessary to generate the magnetisation of CH_2 protons. The apparent dipolar oscillation frequency (3.3 kHz) is appreciably smaller than that observed for the immobile

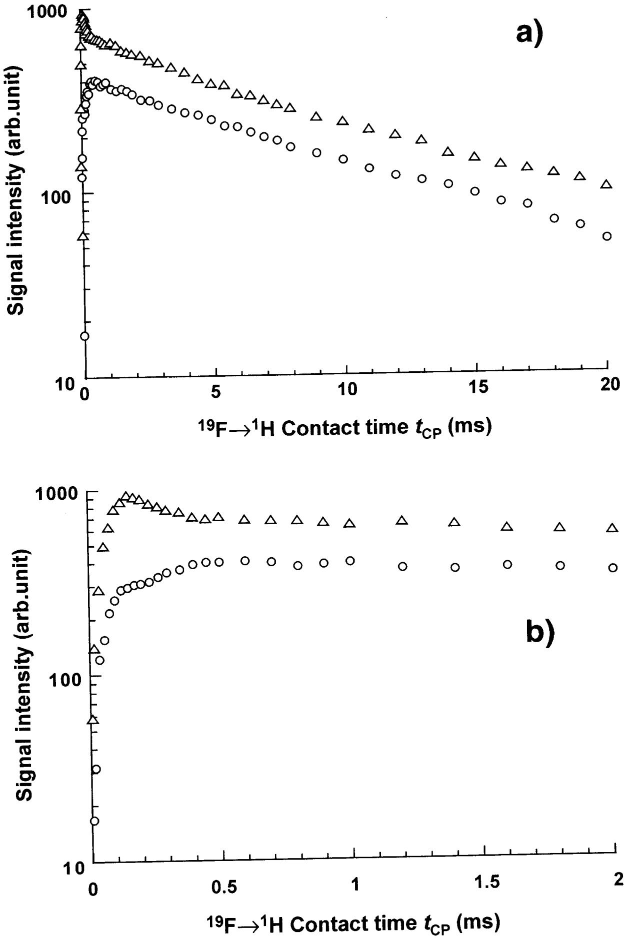

Fig. 17. (a) Contact-time dependence of the ^1H signal intensity for the $^{19}F \rightarrow {}^1H$ CP experiment on PVF, and (b) its magnification for short contact times to show the dipolar oscillation behaviour. This oscillation is observed only for the CHF peak. The oscillation frequency is estimated as 3.3 kHz.

region in the $^1H \rightarrow {}^{19}F$ CP experiment. This probably originates from the fact that CHF signals for the immobile and mobile regions are overlapped in the ^1H spectrum. The dipolar frequency, which corresponds to $r_{HF} = 2.3$ Å, is clearly reduced by motional averaging in the mobile region as is evidenced by a larger dipolar frequency of 5 kHz in the immobile region. When the influence of the oscillation is neglected for the CHF proton, both the CP curves are well fitted by the conventional formula (Eq. (3)) with two effective time constants, T^*_{FH} and $T^*_{1\rho}$. Note that T^*_{FH} and $T^*_{1\rho}$ are effective parameters that characterise the increase and decrease of proton magnetisation. The values thus obtained are $(T^*_{FH}, T^*_{1\rho}) = (0.05, 9.9$ ms) for CHF protons and (0.13, 8.9 ms) for CH_2 protons. The smaller value of T^*_{FH} in the former reflects the relative effectiveness of CP for the CHF group.

3.6. *$^1H \rightarrow {}^{19}F$ CP-drain experiment*

The evolution of residual ^1H magnetisation after $^1H \rightarrow {}^{19}F$ CP can be monitored by the 'CP-drain' experiment which was developed by the authors [11]. The pulse sequence is shown in Fig. 1c. The spectral shape of the residual proton signal after $^1H \rightarrow {}^{19}F$ CP was the same as that of the $^{19}F \rightarrow {}^1H$ CP spectrum, and thus the lineshape was fitted by double Lorentzian functions. Fig. 18 shows the evolution of the ^1H magnetisation obtained from the $^1H \rightarrow {}^{19}F$-CP-drain MAS spectra as a function of t_{CP}. Although this CP-drain curve can be fitted by a double-exponential function as predicted by theory [11], a distinct oscillation was observed for the CHF proton signal in the fast decaying stage. The first dip is observed at 0.16 ms, which is almost the same position as was seen for the CHF proton in the $^{19}F \rightarrow {}^1H$ CP curve. The effective parameters obtained are $(T^*_{HF}, T^*_{1\rho}) = (0.04, 11.9$ ms) for the CHF protons and (0.09, 11.3 ms) for the CH_2 protons. As expected from the theory, the decay rate of the first step ($t_{CP} < 0.2$ ms) of the residual proton magnetisation in the CP-drain curve (0.04 ms for CHF and 0.09 ms for CH_2) coincides with that of the initial increase in fluorine magnetisation in the $^1H \rightarrow {}^{19}F$-CP-curve (0.04–0.08 ms — see Table 1). The decay rate for the second stage ($t_{CP} >$ 0.5 ms) in the CP-drain curve (11.1 ms for CHF and 12.6 ms for CH_2) is also analogous to the decay rate in the CP curve (8.9–13.5 ms). These results indicate that the CP-drain experiment is complementary to the $^1H \rightarrow {}^{19}F$ CP experiment, as expected. In addition, it has been shown that, when the H–H condition is fulfilled, the intercept of the CP-drain curve at $t_{CP} = 0$ is equal to the inverse of $(1 + N_F/N_H)$ (N is the number of spins in unit volume) assuming that $T_{HF}/T^H_{1\rho}$ and $T_{HF}/T^F_{1\rho}$ are very small (these assumptions should be valid considering the large difference between T^*_{HF} and $T^*_{1\rho}$). The value of N_F/N_H thus calculated from the intercept (0.74) is 0.35, which is very close to the value expected from the chemical structure of PVF (0.33). These facts indicate that the CP dynamics behaviour between ^1H and ^{19}F spins in PVF can be acceptably explained in terms of the phenomenological spin thermodynamics theory [11,12] in spite of its two phase (immobile and mobile) nature.

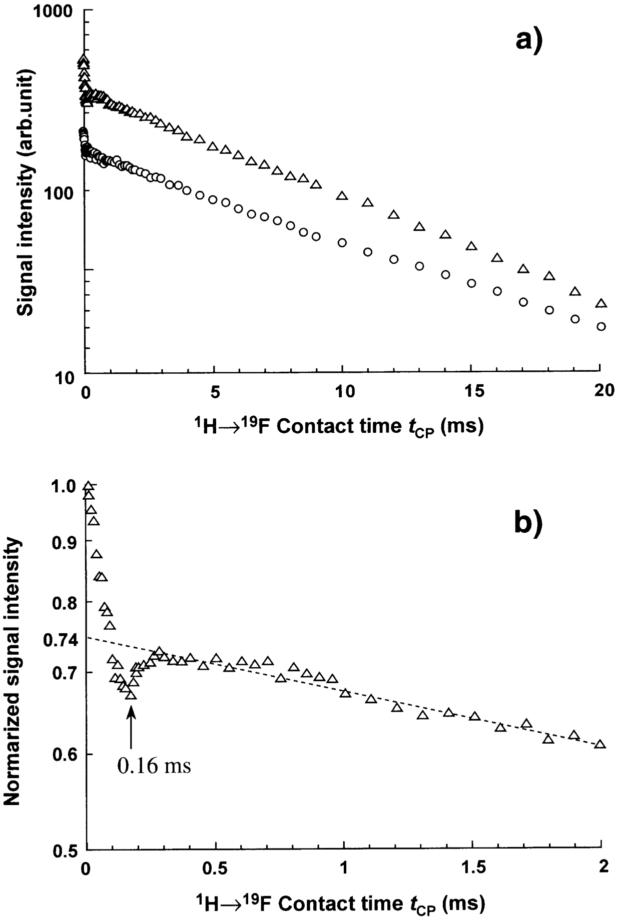

Fig. 18. (a) Contact-time dependence of the ^1H signal intensity for the $^1H \rightarrow {}^{19}F$ CP-drain experiment on PVF, and (b) its magnification for short contact times to show the dipolar oscillation behaviour. The dipolar oscillation is observed only for the CHF peak, and the oscillation frequency is estimated as 3.1 kHz.

4. Conclusions

The solution-state spectrum of PVF dissolved in DMF-d_7 showed a high fraction of the regio-irregular structure (head-to-head units: ca. 11%). The static ^1H pulsed NMR measurements of $T^H_{1\rho}$ and T^H_2 showed the two-phase (immobile and mobile) nature of PVF in the solid state. The variable temperature static broad line ^1H-NMR spectra showed that the onset of the glass transition is estimated as ca. 40°C, but the temperature change of the linewidth occurs smoothly. The static ^1H-NMR experiments using the Goldman–Shen type phase selection at 130°C indicated that a measure for the lamellar size yields about 4.2 nm, assuming reliable spin-diffusion coefficients scaling with the half-height-widths of the spectra of mobile and immobile regions. A high-resolution solid-state ^{19}F spectrum of the mobile region was selectively observed by a newly developed DIVAM pulse sequence using a weak ^{1}H pulse train followed by $^{1}H \rightarrow {}^{19}F$ CP. The spectral shape and the chemical shifts of the mobile region are similar to those observed in the solution-state spectrum. Significant differences in $T_{1\rho}^{F}$ and $T_{1\rho}^{H}$ between the immobile and mobile regions were confirmed by spin-lock experiments in the ^{19}F channel under high-resolution conditions. In addition, the effective time constants, T_{HF}^{*} and $T_{1\rho}^{*}$, which were determined from the $^{1}H \rightarrow {}^{19}F$ CP curves, are also different between the two domains. The effective H···F distance estimated from the dipolar oscillation frequency observed for the CP curves of the immobile region is 2.0 Å, which agrees well with a value for the H–C–F group (2.02 Å) calculated using ab initio MO theory. Such oscillation was not observed for the mobile region in the $^{1}H \rightarrow {}^{19}F$ CP experiment, indicating an absence of effective motional averaging in the immobile region in spite of the imperfections of the crystalline structure. On the other hand, dipolar oscillations were observed also for the mobile region in the $^{1}H \rightarrow {}^{19}F$-IRCP experiment, with significantly smaller oscillation frequencies than that of the immobile region. This difference is straightforwardly ascribed to motion of the polymer chain in the mobile region. Although spinning at 35 kHz is necessary to separate the signals between CHF and CH_2 protons in the ^{1}H MAS spectra, $^{19}F \rightarrow {}^{1}H$ CP-MAS and $^{1}H \rightarrow {}^{19}F$ CP-drain MAS spectra gave complementary information to that from the $^{1}H \rightarrow {}^{19}F$ CP experiment: the effective time constants, T_{HF}^{*}, T_{FH}^{*}, and $T_{1\rho}^{*}$, determined from the former experiments are consistent with those obtained from the latter, and distinct dipolar oscillation was only observed for the signal of CHF proton. This indicates that ^{19}F magnetisation rapidly transfers to the protons in the same CHF group, and then diffuses to those in adjacent CH_2 groups. The value of N_F/N_H calculated from the intercept of the CP-drain curve at $t_{CP} = 0$ (0.35) is consistent with that of the chemical structure of PVF (0.33).

Acknowledgements

One of us (S.A.) is grateful to the Japan Society for the Promotion of Science for a research fellowship in the UK. We also thank B.J. Say, A.M. Kenwright, U. Scheler, G. Hirschinger, and I.H. McKaeg for helpful discussions. Financial support from the UK Engineering and Physical Sciences Research Council under grant GR/L02906 is gratefully acknowledged.

References

[1] Harris RK, Carss SA, Chambers RD, Holstein P, Minoja AP, Scheler U. Bull Magn Reson 1995;17:37.
[2] Holstein P, Scheler U, Harris RK. Magn Reson Chem 1997;35:647.
[3] Holstein P, Harris RK, Say BJ. Solid State Nucl Magn Reson 1997;8:201.
[4] Holstein P, Scheler U, Harris RK. Polymer 1998;39:4937.
[5] Scheler U, Harris RK. Solid State Nucl Magn Reson 1996;7:11.
[6] Monti GA, Harris RK. Magn Reson Chem 1998;36:892.
[7] Isbester PK, Kestner TA, Munson EJ. Macromolecules 1998;31:8192.
[8] Carss SA, Scheler U, Harris RK, Holstein P, Fletton RA. Magn Reson Chem 1996;34:63.
[9] Vierkötter SA. J Magn Reson A 1996;118:84.
[10] Scheler U, Harris RK. Chem Phys Lett 1996;262:137.
[11] Ando S, Reinsberg SA, Harris RK. J Magn Reson 1999;141:91.
[12] Ando S, Reinsberg SA, Harris RK. Magn Reson Chem 1999;37:709–20.
[13] Gorlitz M, Minke R, Trautvetter W, Weisgerner G. Angew Makromol Chem 1973;29/30:168.
[14] Lando JB, Hanes MD. Macromolecules 1995;28:1142.
[15] Brandrup J, Immergut EH, Grulke EA, editors. Polymer handbook 4th ed.. New York: Wiley, 1999.
[16] Aliev AE, Harris KDM. Magn Reson Chem 1994;32:366.
[17] Bruch MD, Bovey FA, Cais RE. Macromolecules 1984;17:2547.
[18] Tonelli AE, Schilling FC, Cais RE. Macromolecules 1981;14:560.
[19] Chen LT, Frank CW. Ferroelectrics 1984;57:51.
[20] Holstein P, Monti G, Harris RK. Phys Chem Chem Phys 1999;1:3549–55.
[21] Kenwright AM, Say BJ. Solid-state proton NMR studies of polymers. In: Ibbett RN, editor. NMR spectroscopy of polymers, Glasgow: Blackie, 1993.
[22] Schmidt-Rohr K, Spiess HW. Multidimensional solid-state NMR and polymers. London: Academic Press, 1994 [chapter 13].
[23] Li S, Chesnut DB. Magn Reson Chem 1985;23:625.
[24] Grover SH, Guthrie JP, Stothers JB, Tan CT. J Magn Reson 1973;10:227.
[25] Müller L, Kumar A, Baumann T, Ernst RR. Phys Rev Lett 1974;32:1402–6.
[26] Naito A, McDowell CA. J Chem Phys 1986;84:4181.
[27] Reinsberg SA, Ando S, Harris RK. Polymer 2000;41:3729.
[28] Reinsberg SA. MSc Thesis. University of Durham; 1998.
[29] Ovenall DW, Uschold RE. Macromolecules 1991;24:3235.